

# Monte Carlo simulation of colloidal membrane filtration: Model development with application to characterization of colloid phase transition

Jim C. Chen<sup>a</sup>, Menachem Elimelech<sup>a</sup>, Albert S. Kim<sup>b,\*</sup>

<sup>a</sup> Department of Chemical Engineering, Environmental Engineering Program, Yale University, P.O. Box 208286, New Haven, CT 05620-8286, USA

<sup>b</sup> Department of Civil and Environmental Engineering, University of Hawaii at Manoa, Honolulu, HI 96822, USA

Received 22 November 2004; received in revised form 10 February 2005; accepted 14 February 2005

Available online 19 March 2005

## Abstract

This study investigates phase transition from a fluid-like polarization layer to a solid cake layer of particle deposits during membrane filtration of interacting colloidal particles. A Monte Carlo simulation model of dead-end filtration is used under the influences of hydrodynamic bias from the permeation flux as well as inter-particle interactions. The model effectively demonstrates the roles of the hydrodynamic drag force and inter-particle potential in governing the volume fraction of the particle deposit. The cake layer volume fraction is shown to be sensitive to the combination of particle surface (zeta) potential, solution ionic strength, particle size, and applied transmembrane pressure. Further application of the model leads to a holistic characterization of the phase transition phenomenon. The onset of phase transition is characterized with flexibility and adaptability with concern for both physico-chemical standards, such as volume fraction and inter-particle separation distance, as well as pragmatic considerations, such as the desire to operate the system below the critical flux and avoidance of irreversible cake formation.

© 2005 Elsevier B.V. All rights reserved.

**Keywords:** Monte Carlo simulation; Hydrodynamic bias; Colloidal membrane filtration; Phase transition; Critical flux

## 1. Introduction

The phase transition from fluid to solid of particles deposited onto a membrane surface during filtration poses an important fundamental subject of investigation in the operation of membrane separation processes. The solidification of the particle deposit incurs significant practical and economic ramifications. The formation of a cake layer of particles on the membrane surface directly causes a phenomenon, termed membrane fouling, which results in precipitous decline in the permeation flux through the membrane. Therefore, the efficiency of membrane filtration is greatly impaired by the presence of a solid cake deposit. Optimal operation of a membrane unit seeks to avoid fouling by working under the point

of phase transition, namely the initiation of a colloidal cake layer [1,2]. Presently, the exact delineation of the point of phase transition remains an open question with a number of proposed methods for its characterization [3]. The purpose of this study is to investigate the phase transition phenomenon associated with membrane fouling using a Monte Carlo simulation model of colloidal transport and interaction in membrane filtration.

To arrive at a holistic understanding of the intricate processes of colloidal transport in membrane filtration necessitates a breaking down of this multiplexed problem into individual contributions of fundamental physical processes that comprise the overall system. Several physical phenomena operate cooperatively and competitively in a typical filtration system to generate the observed permeate flux behavior. Among them, two opposing forces that play prominent roles in affecting the system response are hydro-

\* Corresponding author. Tel.: +1 808 956 3718; fax: +1 808 956 5014.  
E-mail address: [albertsk@hawaii.edu](mailto:albertsk@hawaii.edu) (A.S. Kim).

dynamic drag and inter-particle electrostatic repulsion [4]. Both forces act discretely on each individual particle while experiencing many-body interferences from the neighboring particles. So, within a suspension of colloids, a complex network of counteracting forces will arise and will represent one of the most crucial components of the system. Each of the forces should be accurately described in order to develop a consummate simulation model of colloidal membrane filtration.

To do so, an ideal model should then narrow its scope to a microscopic scale and meticulously compute each distinct force and displacement. A macroscopic approach offers an expedient alternative by integrating the sum of the forces. However, the trade-off for an integral method is that it bypasses the opportunity to investigate the system behavior in minute detail [5–7]. A microscopic model, on the other hand, offers the advantage of pinpointing definitively the forces that account for each individual observed system response [8]. Such a modeling approach affords precise definition of every physical dynamic that is at work. The many-body composition of colloidal systems renders it to be especially suitable for a microscopic modeling technique.

The current study applies the Monte Carlo simulation method for microscopic modeling of colloidal transport in membrane filtration. Monte Carlo simulation utilizes a stochastic modeling strategy that first selects discrete particle displacements with statistical randomness and then evaluates each selection on the basis of its physical validity. The model will accept those proposed displacements that qualify as being physically legitimate and disqualify physically unreasonable ones. As the simulation proceeds, the model generates a pool of statistically random, discrete, microscopic particle movements from which it maps each particle trajectory. The Monte Carlo method has traditionally proven itself to be a powerful modeling application across a myriad of scientific and mathematical disciplines [8,9]. The emergence of the Monte Carlo method in membrane filtration research remains in its burgeoning stage. It is our aspiration for this paper to contribute to the sustaining growth of the Monte Carlo method as a viable modeling alternative in the research of membrane separation processes and also to apply it to further understand the critical phase transition phenomenon occurring during colloidal membrane filtration.

## 2. Definition of system for modeling

### 2.1. Overview of membrane filtration systems

Fig. 1 shows examples of membrane filtration systems operating in the typical dead-end and crossflow modes along with an outline of the important forces to consider. In the dead-end mode of operation (Fig. 1(a)), the applied pressure within the system imposes a downward permeation drag force that propels particles to accumulate on the membrane

surface. The formation of the particle deposit is stratified into two regions, a fluid polarized layer situated above a compact cake layer below. When an additional fluid flow in the horizontal direction is added, the mode of operation becomes the crossflow type as shown in Fig. 1(b). Here, the particles still will accumulate on the membrane surface during filtration, while the added crossflow now serves to afford the particle deposit another degree of movement along the horizontal direction.

Fig. 1(c) shows a more introspective breakdown of the combination of forces acting together in the system. Hydrodynamic drag in the downward direction promotes particle deposition onto the membrane surface to initially form a polarized layer of highly concentrated suspension and then continues to further induce solidification of the polarized layer to form a compact cake layer below it (Fig. 1(a) and (b)). Conversely, inter-particle interactions, in particular electrostatic repulsion, mollify particle consolidation and create a more porous cake layer. Moreover, particles may coagulate into aggregate form with adhesion to one another prior to their deposition onto the membrane surface. Under these conditions, the cake layer formation dynamics may entail a two-stage progression where the initial deposit on the membrane surface is a porous coagulated substructure which then undergoes a second stage of compression and restructuring to reach the final cake layer configuration. Such a dual-stage formation is observed experimentally in Tarabara et al. [10]. The gravitational compressive force (Fig. 1(c)) occurs as the net resultant of the sum of all accumulated particles positioned above a particular location in the cake layer. Furthermore, particles once deposited may restructure their configuration. Restructuring may be traceable to a number of possible causes. Among them is the deflection of the downward hydrodynamic drag and compressive forces so as to induce lateral movement of particles. The deflection of forces arises due to the complex interactions of many forces operating within a many-body particle configuration. When dealing with a crossflow filtration system, the crossflow shear introduces another source of restructuring dynamics whereby particles flow laterally across the membrane surface and possibly become re-entrained into bulk suspension [8,11–13]. Other important considerations include aggregate breakage, inelastic particle collisions (Fig. 1(c)), and time dependent issues such as the implications of a slow cake development in dilute suspensions with singular particle deposition as compared to the rapid case at high concentrations with particles depositing in clusters [14,15].

So, colloidal membrane filtration encompasses a complex network of counteracting physical processes that calls for a microscopic modeling technique to accurately and precisely describe the system. The purpose of this study is to present a Monte Carlo simulation model of particle deposition dynamics during membrane filtration. We will focus on the issues pertinent to the fundamental algorithms and parameters for developing the model. Two of the primary forces

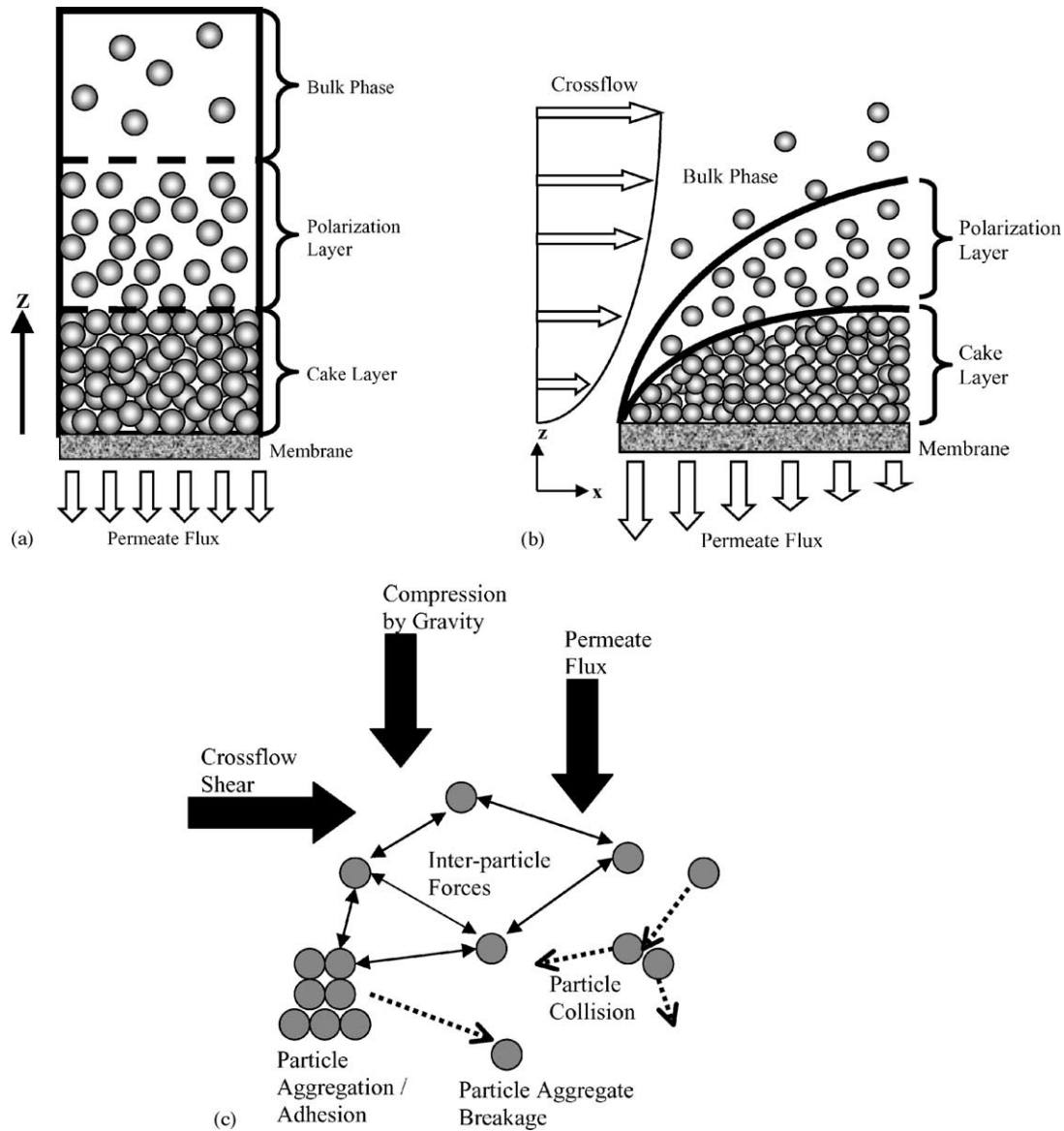


Fig. 1. (a) Schematic of a dead-end filtration system, (b) schematic of a crossflow filtration system, and (c) outline of forces driving colloidal transport, aggregation, and breakage.

shown in Fig. 1(c), the downward hydrodynamic drag and the inter-particle interactions, will be incorporated into the model. The model will then be applied to investigate the phase transition phenomenon of the polarized layer from fluid to solid. We will relate the observation of a point of critical flux during filtration to the occurrence of phase transition. Multiple possible definitions of critical flux are available and we will explore the applicability of each [16,17]. The significance of each proposed point of phase transition in relationship to membrane filtration performance will be examined.

Further extensions from the current model to include the complete set of forces as shown in Fig. 1(c) will culminate in a complete Monte Carlo simulation model that remains true to the actual physical situation and can effectively investigate

significant issues such as phase transition during crossflow filtration, among others.

## 2.2. Governing equations for the system

### 2.2.1. Equations for mass transport

The governing equation for colloidal transport in a dead-end filtration system is [5,18]:

$$\frac{\partial \phi}{\partial t} = \frac{\partial}{\partial z} \left( D(\phi) \frac{\partial \phi}{\partial z} - v\phi \right) \tag{1}$$

with boundary condition:

$$\phi = \phi_b \text{ at } t = 0, \quad \phi = \phi_b \text{ at } z = \delta_{cp},$$

$$D(\phi_m) \frac{\partial \phi}{\partial z} = v\phi_m \text{ at } z = 0 \quad (2)$$

where  $\phi$  is the volume fraction of particles,  $\phi_b$  the bulk volume fraction,  $\phi_m$  the particle volume fraction on the membrane surface,  $D(\phi)$  the concentration-dependent diffusion coefficient of particles [19],  $t$  the time,  $z$  the axis perpendicular to the membrane surface,  $\delta_{cp}$  the thickness of the polarization layer, and  $v$  the permeate flux.

Likewise for a crossflow system the governing equation for mass transport becomes [5,18]:

$$u \frac{\partial \phi}{\partial x} = \frac{\partial}{\partial z} \left( D(\phi) \frac{\partial \phi}{\partial z} - v\phi \right) \quad (3)$$

with boundary conditions:

$$\phi = \phi_b \text{ at } z = \delta_{cp}, \quad \phi = \phi_b \text{ at } x = 0,$$

$$D(\phi_m) \frac{\partial \phi}{\partial z} = v\phi_m \text{ at } z = 0 \quad (4)$$

where  $u$  is the additional crossflow velocity in the axial,  $x$ , direction. It should be noted from a comparison of Eqs. (1) and (3) that dead-end filtration is inherently a time-dependent, transient process while crossflow filtration will reach a time-independent steady state of operation. The boundary condition given in Eq. (4) applies for the case of the polarization layer in the absence of cake formation.

### 2.2.2. Equations for filtration

In general, one of the quantities of special interest in applications of membrane filtration is the permeate flux which, for both dead-end and crossflow filtration (after cake formation has occurred), is governed by Darcy's Law [20]:

$$v_w = -v = \frac{\Delta P}{\mu(R_m + R_c)} \quad (5)$$

where  $v_w$  is the permeate flux in magnitude,  $\Delta P$  the applied pressure within the system,  $\mu$  the absolute fluid viscosity,  $R_m$  the membrane resistance, and  $R_c$  the cake layer resistance further defined as

$$R_c = r_c \delta_c, \quad r_c = \frac{9\phi_c}{2a^2} \Omega \quad (6)$$

where  $r_c$  is the specific cake resistance,  $\delta_c$  the cake layer thickness,  $a$  the particle radius,  $\phi_c$  the cake layer volume fraction and  $\Omega$  the Happel's correction factor defined as [21]:

$$\Omega = \frac{1 + \frac{2}{3}\phi^{5/3}}{1 - \frac{3}{2}\phi^{1/3} + \frac{3}{2}\phi^{5/3} - \phi^2} \quad (7)$$

The model presented in this study will utilize MC simulation to compute the volume fraction to be inputted into Eqs. (1)–(7) under given operating conditions to obtain the system response.

## 2.3. Interaction forces in membrane filtration

### 2.3.1. Inter-particle interaction

One of the principal input parameters to the model is the inter-particle interaction potential. In the current study, the inter-particle potential is modeled by DLVO theory [22,23]:

$$V_{TOT} = V_{VDW} + V_{EDL} \quad (8)$$

where  $V_{VDW}$  is the van der Waals' potential and  $V_{EDL}$  the electrostatic double layer potential. The attractive van der Waals' potential between equal-sized particles can be modeled by many available expressions. In this study, it is calculated by [24]:

$$V_{VDW} = -\frac{A_H}{12} \left[ \frac{4}{s^2} + \frac{4}{s^2 - 4} + 2 \ln \left( 1 - \frac{4}{s^2} \right) \right] \quad (9)$$

where  $A_H$  is the Hamaker constant and  $s = r/a$  the dimensionless center-to-center separation between two particles scaled by the particle radius  $a$ .

The electrostatic interaction potential between the particles is calculated from the linear superposition approximation of Bell et al. [25] and Chew and Sen [26]:

$$V_{EDL} = \frac{128 \pi n_0 a \gamma^2 k_B T e^{-\kappa a (s-2)}}{\kappa^2 s} \quad (10)$$

$$\gamma = \tan h \left( \frac{z_s e \psi_s}{4 k_B T} \right) \quad (11)$$

$$\kappa^{-1} = \sqrt{\frac{\epsilon_r \epsilon_0 k_B T}{2e^2 z_s^2 n_0}} = \sqrt{\frac{\epsilon_r \epsilon_0 k_B T}{2000 e^2 N_A I}} \quad (12)$$

where  $\kappa^{-1}$  is the Debye screening length,  $N_A$  the Avogadro's number,  $I$  the ionic strength of the solution,  $\epsilon_r$  the dimensionless dielectric permittivity of water,  $\epsilon_0$  the permittivity of free space,  $n_0$  the ion number concentration,  $k_B$  the Boltzmann's constant,  $T$  the absolute temperature,  $z_s$  the valence of ions in the bulk solution,  $e$  the charge of an electron, and  $\psi_s$  the surface potential of the particles which can be substituted by the zeta potential [27].

### 2.3.2. Hydrodynamic drag force

The second primary physical parameter inputted into the current model is the hydrodynamic drag. The expression for the hydrodynamic drag force derives directly from Stoke's law for a single particle in an infinitely unbounded medium:

$$F_{Stokes} = 6\pi\mu av \quad (13)$$

where  $\mu$  is the fluid viscosity and  $v$  the permeate velocity. For fluid flow through a porous medium composed of equal-sized spherical particles, the true hydrodynamic drag force exerted on each particle within the medium is adjusted by Happel's correction factor  $\Omega$ , defined earlier in Eq. (7), [19]:

$$F_{hydro} = F_{Stokes} \Omega \quad (14)$$

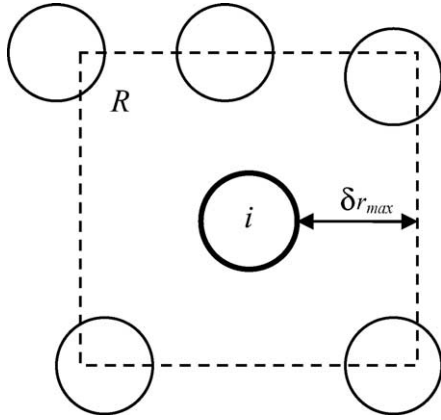


Fig. 2. Range of particle displacements for Monte Carlo simulation.

### 3. Monte Carlo simulation method

#### 3.1. Background on Monte Carlo method

Monte Carlo simulation (MC) is a stochastic modeling method that is especially suitable to problems involving the dynamics of particle motion because of its capability to evaluate each discrete particle displacement. A classical method for performing MC begins by casting the process as being Markovian, meaning that the outcome for a particle displacement depends solely on the outcome that immediately precedes it. The system progresses from one state to the next by aid of its transition probability matrix. Metropolis et al. [28] present the now standard Metropolis method for conducting MC simulations using the energy of the system as the criterion to evaluate the acceptance or rejection of a MC step.

The Metropolis method begins by considering a system of particles as shown in Fig. 2. The particle of interest  $i$  is initially located at  $r_i^m$ . Particle  $i$  is then proposed to be displaced randomly to a new location  $r_i^n$  using the algorithm:

$$r_i^n = r_i^m + (2a_0 - 1)\delta r_{\max} \quad (15)$$

where  $a_0$  is a uniform random number between 0 and 1 and  $\delta r_{\max}$  the maximum allowable displacement. The proposed displacement is next evaluated for acceptance or rejection. The criterion for acceptance is the change in potential energy  $\Delta V_{n,m}$  of the system computed as

$$\Delta V_{n,m} = \sum_{j \neq i}^N V(r_{i,j}^n) - \sum_{j \neq i}^N V(r_{i,j}^m) \quad (16)$$

If  $\Delta V_{n,m} < 0$ , then the proposed move is downhill and accepted. If  $\Delta V_{n,m} > 0$ , the proposed move is uphill and is accepted with the qualification of the probability  $\rho_n/\rho_m$  which in the Metropolis method corresponds to the Boltzmann factor of the energy difference:

$$\frac{\rho_n}{\rho_m} = \frac{\exp(-\beta V_0) \exp(-\beta \Delta V_{n,m})}{\exp(-\beta V_n)} = \exp(-\beta \Delta V_{n,m}) \quad (17)$$

where  $\beta = 1/k_B T$ . In this procedure, a uniform random number between 0 and 1,  $\xi$ , is generated and compared with  $\exp(-\beta \Delta V_{n,m})$ . If  $\xi < \exp(-\beta \Delta V_{n,m})$ , then the uphill move is accepted. Otherwise the proposed move is rejected for  $\xi > \exp(-\beta \Delta V_{n,m})$ . The overall effect is that the particle proceeds with changes in potential energy  $\Delta V_{n,m}$  accepted with probability  $\exp(-\beta \Delta V_{n,m})$ . If the uphill move is rejected, the particle remains in its original position, and the non-move is taken to be a new state nevertheless.

The modeling procedure continues by randomly selecting successive particles for proposed displacements and evaluating each move. Hastings [29] presents an equally valid method of selecting particles systematically according to their indices rather than by random selection. This step eases the number of random number generations. For the Hastings method, an important distinction should be noted, and that is it does not satisfy detailed balance. Manousiouthakis and Deem [30] prove that the Hastings method only satisfies balance. Details of Monte Carlo modeling are given in Allen and Tildesley [9].

#### 3.2. Hydrodynamic bias Monte Carlo simulation algorithm for colloidal membrane filtration

The model in the current study utilizes a rectangular simulation box containing 1024 particles. The algorithm for the simulation follows the method described in Section 3.1. Individual particles are assigned random proposed displacement with subsequent evaluation of the energy change of each move. Downhill moves ( $\Delta V < 0$ ) are readily accepted while uphill moves are subject to the probability test given in Eq. (17).

A preliminary MC simulation is first performed to obtain an equilibrium configuration for the particles. Details of this procedure are given in Kim and Hoek [31]. Upon reaching an equilibrium configuration, the simulation proceeds to model particle motion under the influences of hydrodynamic drag and inter-particle interaction potential. It is important to note here that the particles should be displaced solely in one of the three orthogonal directions ( $x$ ,  $y$ , and  $z$  only) for each energy evaluation (Fig. 3). This stipulation ensures that forces acting in a perpendicular direction to the proposed particle

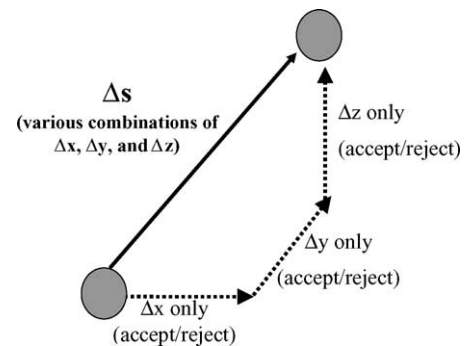


Fig. 3. Sequence of particle displacements during Monte Carlo simulation.

displacement will not affect that particular particle move. So, the hydrodynamic drag force, which acts in the downward  $z$ -direction, will only come into play when particles are displaced solely in the  $z$ -direction and will not influence particle motion in the  $x$ - or  $y$ -directions only. Such a vectorial decomposition offers faster convergence to the dynamic equilibrium of the system. The randomness of the displacement selections is maintained to be almost identical to the case without the decomposition. This procedure results in a mean field hydrodynamic bias MC method.

When particles are displaced in the  $x$  or  $y$  directions only, the expression for the energy evaluation is

$$\Delta V_{x,y} = V_{\text{TOT,NEW}} - V_{\text{TOT,OLD}} \quad (18)$$

where the total inter-particle interaction energy  $V_{\text{TOT}}$  is computed according to Eqs. (8)–(12). The added subscripts NEW and OLD signify total inter-particle energy computed at the proposed displacement location and at the original particle location, respectively.

Particle displacements in the  $z$ -direction only will acquire an additional term in the energy evaluation due to the downward hydrodynamic drag force. The expression for the difference in energy then becomes:

$$\Delta V_z = V_{\text{TOT,NEW}} - V_{\text{TOT,OLD}} + F_{\text{Stokes}}\Omega(z_{\text{new}} - z_{\text{old}}) \quad (19)$$

where  $z_{\text{new}}$  and  $z_{\text{old}}$  are the  $z$  coordinates of particles at the proposed displacement and original locations, respectively. For particle motion in the  $z$ -direction, there is no cyclic boundary condition occurring at the membrane surface. Particles are not allowed to move below  $z = 0$ . For cases involving a cyclic boundary condition, the simulation step must maintain balance [9,30]. The simulation proceeds with individual particle displacements followed by energy evaluations according to Eqs. (18) and (19) until reaching a final dynamic equilibrium particle configuration. The criterion for ascertaining equilibration of the system is that the volume fraction of the cake layer and average inter-particle separation between a pair of nearest particles reach a steady state and remain constant continuously after that point. Details of this bias Monte Carlo technique are verified and well discussed in Kim et al. [32].

## 4. Results and discussion

### 4.1. Influence of hydrodynamic drag and inter-particle interactions on cake layer volume fraction

Fig. 4 shows the model results that simulate the deposition of particles at the membrane surface under the coupled influences of hydrodynamic drag and inter-particle electrostatic interaction. The specific input parameters used in these simulations are given in Table 1. In Fig. 4, the volume fraction of the particle deposit is given as a function of observed permeate flux of the filtration system. In these simulations, a

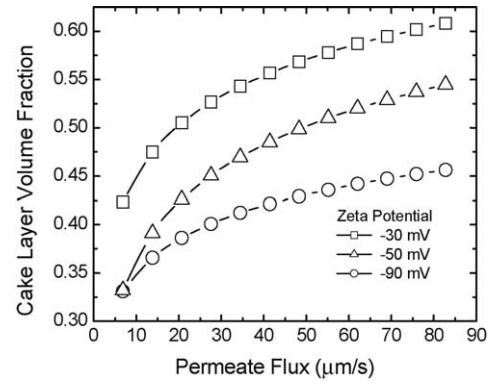


Fig. 4. Cake layer volume fraction in relation to permeate flux with varying zeta potential. The following parameters (in addition to those listed in Table 1) were used in the simulations: particle radius = 100 nm, ionic strength =  $10^{-3}$  M.

permeate flux is first set to a selected value. Then, the effective permeate flux within the cake layer is adjusted for the volume fraction of the porous medium according to Eq. (12) to yield the actual hydrodynamic drag force experienced by the particles. The model utilizes the adjusted hydrodynamic drag force along with the inter-particle potential to simulate particle deposition and the final cake configuration. Each curve in Fig. 4 essentially shows the increase in volume fraction of particles with increasing compressive force from the adjusted hydrodynamic drag. For instance, at  $-30$  mV zeta potential, the cake layer volume fraction increases from 0.423 to 0.608 with corresponding increases in the observed permeate flux from 6.9 to 82.8  $\mu\text{m/s}$ . Conversely, increasing the particle zeta potential effectively strengthens the inter-particle electrostatic repulsion and prevents particles from closely approaching one another (low volume fraction). At zeta potential of  $-90$  mV, the cake layer attains a volume fraction of only 0.456 at observed permeate flux of 82.8  $\mu\text{m/s}$ , contrasted to a much greater volume fraction of 0.608 for  $-30$  mV.

Similar trends are shown in Fig. 5 for cake layer formation under various solution ionic strengths. Like the zeta potential, the solution ionic strength governs the magnitude and range of the inter-particle electrostatic interaction. At high ionic strength, excess electrolyte ions screen the inter-particle interactions and lessen the inter-particle repulsion. For instance, at an ionic strength of  $10^{-2}$  M, the cake layer volume fraction is shown to be consistently higher than that for  $10^{-4}$  M. However, it is interesting to note that, for all three ionic strengths at observed permeate flux 82.8  $\mu\text{m/s}$ , the cake layer volume fractions converge to a value of ap-

Table 1  
Operating and system conditions for model simulations

Hamaker constant, $A_H$ (J)	$4.6 \times 10^{-21}$
Valence of ions, $z_s$	1
Dielectric permittivity of water	78.54
Permittivity of free space ( $\text{C}^2/\text{N m}^2$ )	$8.854 \times 10^{-12}$
Temperature (K)	298.5
Membrane resistance (1/m)	$1 \times 10^{12}$

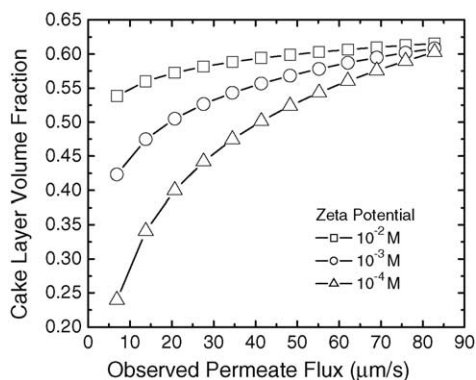


Fig. 5. Cake layer volume fraction in relation to permeate flux with varying solution ionic strength. The following parameters (in addition to those listed in Table 1) were used in the simulations: particle radius = 100 nm, zeta potential =  $-30$  mV.

proximately 0.6, the random loose packing ratio according to Onoda and Liniger [33]. The hydrodynamic drag dominates the influence from the ionic strength at this point. The results of Figs. 4 and 5 demonstrate the model's capacity to successfully capture the compelling and contrary impact of hydrodynamic drag and inter-particle electrostatic interaction on cake layer formation. Comparison of Figs. 4 and 5 reveals that the zeta potential serves as a stronger differentiating agent over the ionic strength for cake formation dynamics at high permeate flux as the profound impact of zeta potential remains clearly evident at high permeate flux.

The consolidation of the particles is visually apparent in Fig. 6. Note that the point of view in Fig. 6(a)–(c) spans from the membrane surface to the bulk in the positive  $z$ -direction. Take, for instance, the case of particle zeta potential  $-30$  mV. With an observed permeate flux of  $6.9 \mu\text{m/s}$ , the particles remain sparsely concentrated (volume fraction = 0.423), and an appreciable average center-to-center nearest pair inter-particle spacing of 2.250 times particle radius is clearly discernible. Upon increasing the observed permeate flux to  $27.6 \mu\text{m/s}$ , the volume fraction rises accordingly to a value of 0.527 with average inter-particle spacing of 2.075 times radius. The particles are consolidating but still not yet in contact with one another. A comparison of Fig. 6(a) and (b) reveals the noticeable compression of the particles and reduction in inter-particle spacing due to heightened hydrodynamic drag. Finally, the particles contact one another when the observed permeate flux reaches  $82.8 \mu\text{m/s}$  as seen in Fig. 6(c), with average center-to-center inter-particle spacing of 2.002 times particle radius (i.e., particle contact). The volume fraction of 0.608 at this point suggests that the particles are configured in random packing [33]. The illustration given in Fig. 6 captures well the randomness of the particle configuration.

The role of inter-particle repulsion can be seen for the case of  $-90$  mV in Fig. 7. In this case, the cake layer volume fraction at permeate flux  $6.9 \mu\text{m/s}$  is 0.331 with sparse average center-to-center inter-particle spacing of 2.450 times particle radius. The volume fraction compresses to only 0.456 with average inter-particle spacing 2.175 times particle radius at

$82.8 \mu\text{m/s}$ . The particles do not come into contact despite the relatively high permeate velocity. The more porous cake structure formed at the higher zeta potential is visibly evident.

Besides showing the effects of increasing hydrodynamic drag force, the progression depicted in Fig. 6 provides one possible answer to the question of phase transition. *The polarized layer of colloidal particles near the membrane surface progressively consolidates under increasing hydrodynamic drag force to reach a point of contact among the particles. The point of particle contact delineates the onset of a solid phase. The volume fraction of particles need not reach ordered maximum packing but only random maximum packing.*

The definition of phase transition given above proceeds directly from inspection of the inter-particle spacing. It is straightforward and simplistic, but does not include practical considerations that will furnish it to be more pertinent to the operations of membrane filtration systems. The definition of phase transition will be addressed with greater refinement and sophistication in Section 5, with inclusion of concepts of critical flux and cake reversibility.

The prominent roles that the hydrodynamic drag force and inter-particle electrostatic interaction play in cake layer formation are definitely evident in Figs. 6 and 7. Therefore, it becomes imperative for any simulation model to accurately characterize these two quantities. This crucial step in the development of the model will be discussed in greater detail in Section 4.3.

#### 4.2. Sensitivity of cake volume fraction to particle size

Fig. 8 shows the model results for simulations of different sizes of particles. As the hydrodynamic drag force is a function of the particle radius according to Eq. (13), it would follow that a smaller particle radius would then produce particle configurations of lower volume fraction. For instance at  $82.8 \mu\text{m/s}$  permeate flux, the particle volume fraction drops off from a value of 0.659 for 200 nm particles to 0.489 for 50 nm particles. So, the particle radius proves to be another important model parameter. The need to accurately size the model particles stands without question. However, implications of the sensitivity of the particle configuration to the radius pervades to other deeper issues.

For filtration of polydisperse suspensions, one belief about the polydisperse particle size distribution states that the smaller particles will occupy void spaces between the larger ones and thereby increase the overall volume fraction [34,35]. However, this notion should be conditioned by the observation that particles of various sizes will experience different hydrodynamic drag forces. So, the deposition dynamics of particles will vary according to the particle sizes. Therefore, the possibility exists that within the cake layer there may be a disproportionate particle size distribution that is different from the distribution in the bulk phase. Instead of the situation with void-filling by smaller particles, the cake layer may exhibit a stratification with respect to particle size where the larger particles are abundant throughout and smaller parti-

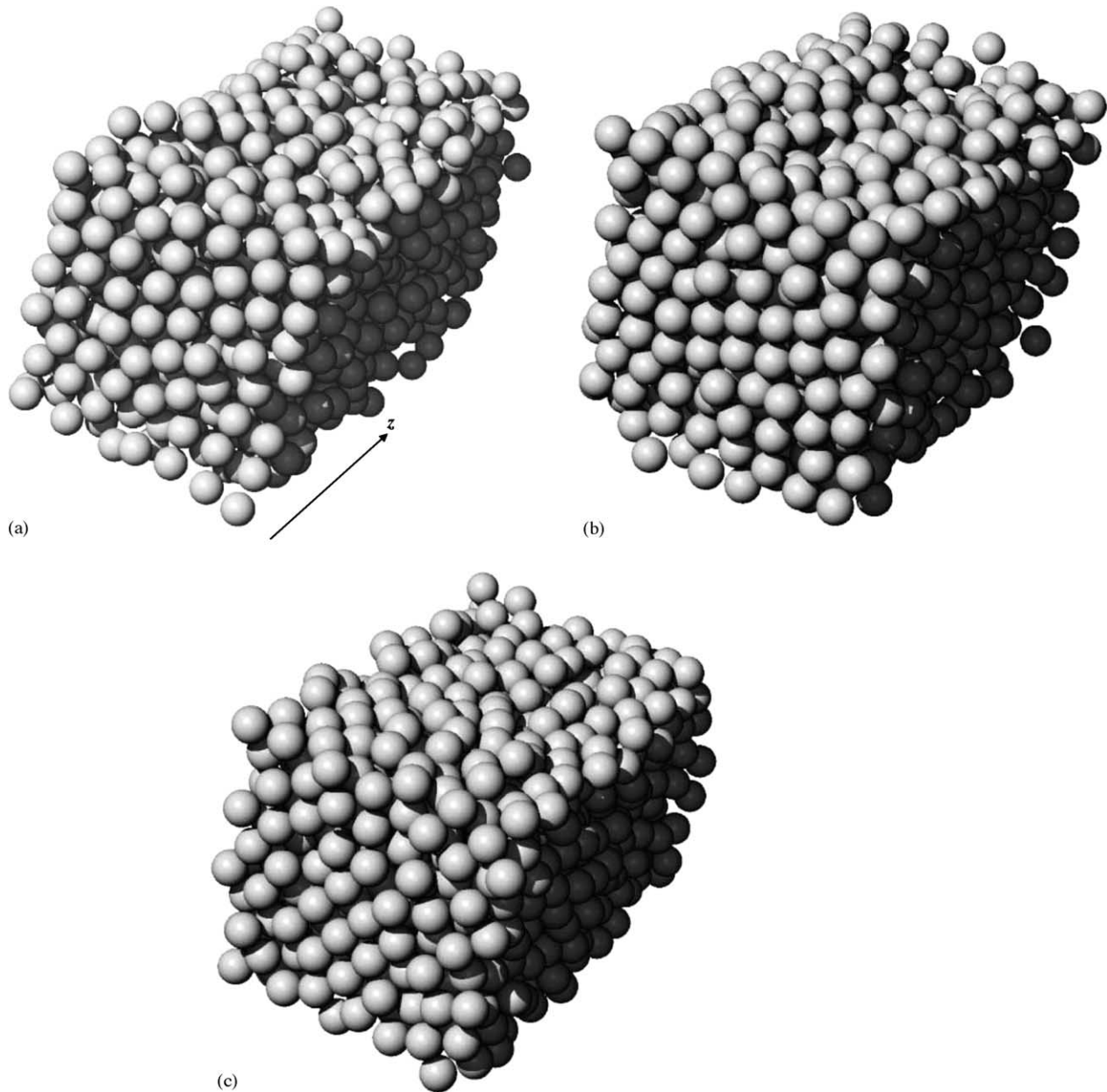


Fig. 6. Illustrations of final particle configurations. (a) Observed permeate flux =  $6.9 \mu\text{m/s}$ , particle radius =  $100 \text{ nm}$ , ionic strength =  $10^{-3} \text{ M}$ , zeta potential =  $-30 \text{ mV}$ , volume fraction =  $0.423$ , average center-to-center inter-particle spacing =  $2.250$  times particle radius. (b) Observed permeate flux =  $27.6 \mu\text{m/s}$ , particle radius =  $100 \text{ nm}$ , ionic strength =  $10^{-3} \text{ M}$ , zeta potential =  $-30 \text{ mV}$ , volume fraction =  $0.527$ , average inter-particle spacing =  $2.075$  times particle radius. (c) Observed permeate flux =  $82.8 \mu\text{m/s}$ , particle radius =  $100 \text{ nm}$ , ionic strength =  $10^{-3} \text{ M}$ , zeta potential =  $-30 \text{ mV}$ , volume fraction =  $0.608$ , average inter-particle spacing =  $2.002$  times particle radius.

cles deposit mostly near the top portions of the cake layer. Now the smaller particles contribute not a void-filling effect but only a higher specific resistance within a certain concentrated region in the cake layer.

In addition, complications will arise in crossflow filtration of polydisperse particles. Here, the larger particles will experience greater hydrodynamic drag from the crossflow and be more susceptible to re-entrainment back into the bulk. The tendency for the larger particles to re-entrain will work

against its faster downward velocity. So, once again, the situation portrays a complex counteraction between two hydrodynamic drag forces, permeation and crossflow, both of which are functions of a polydisperse particle distribution. This may then explain the contradictory findings intimated in some studies that the crossflow functions to reduce the permeate flux [11,36] when the traditional view contends just the opposite. Thus, a macroscopic generalization of the system response to variations in particle sizes is open to exceptions

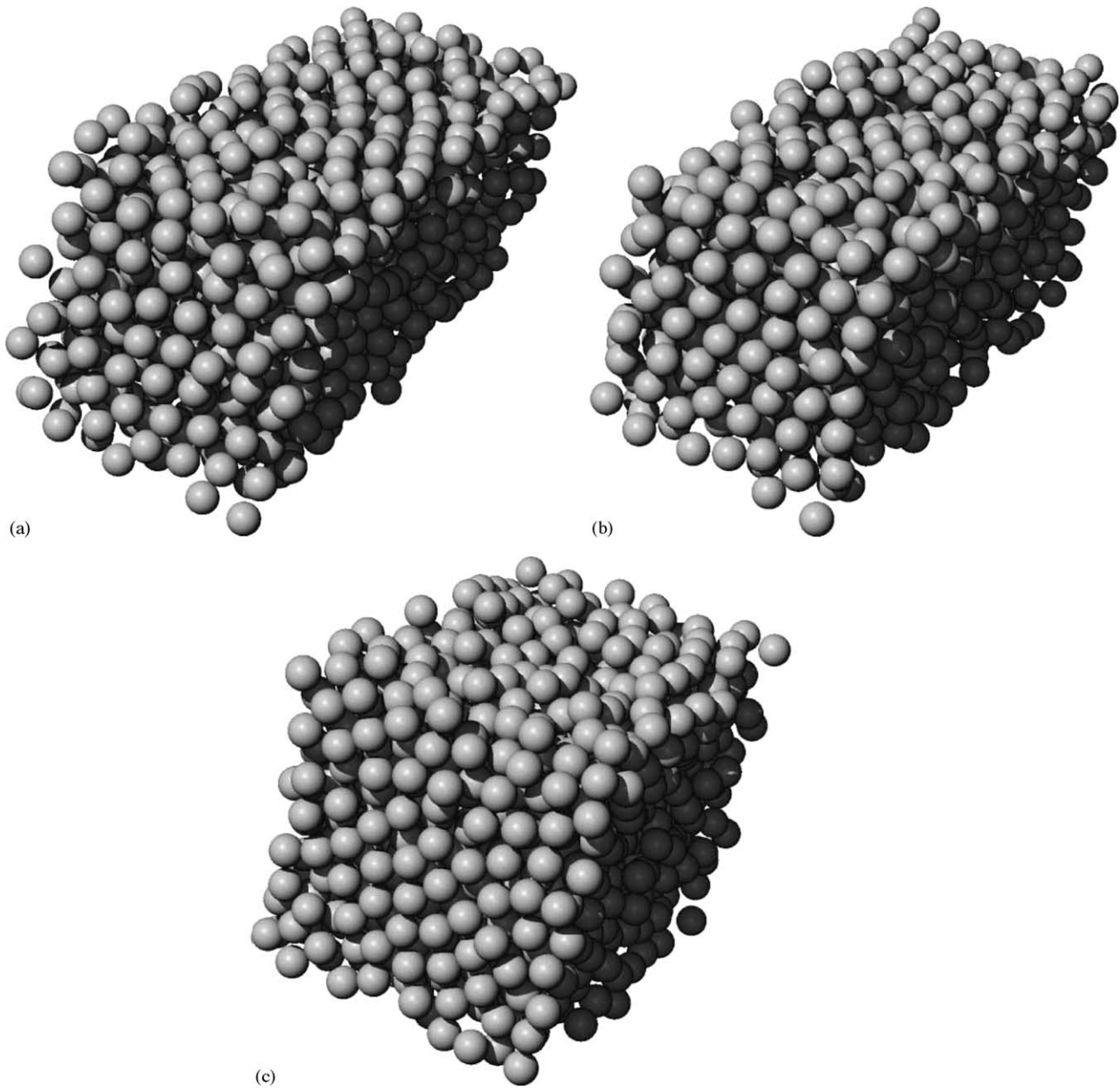


Fig. 7. Illustrations of final particle configurations. (a) Observed permeate flux =  $6.9 \mu\text{m/s}$ , particle radius =  $100 \text{ nm}$ , ionic strength =  $10^{-3} \text{ M}$ , zeta potential =  $-90 \text{ mV}$ , volume fraction =  $0.331$ , average center-to-center inter-particle spacing =  $2.450$  times particle radius. (b) Observed permeate flux =  $27.6 \mu\text{m/s}$ , particle radius =  $100 \text{ nm}$ , ionic strength =  $10^{-3} \text{ M}$ , zeta potential =  $-90 \text{ mV}$ , volume fraction =  $0.401$ , average inter-particle spacing =  $2.250$  times particle radius. (c) Observed permeate flux =  $82.8 \mu\text{m/s}$ , particle radius =  $100 \text{ nm}$ , ionic strength =  $10^{-3} \text{ M}$ , zeta potential =  $-90 \text{ mV}$ , volume fraction =  $0.456$ , average inter-particle spacing =  $2.175$  times particle radius.

as those observed in Mackley and Sherman [11,36]. But, a microscopic model such as MC simulation is sufficiently robust to capture such anomalies by rigorously computing each individual particle trajectory.

#### 4.3. Selection of model parameters

Figs. 4, 5 and 8 have clearly demonstrated the considerable impact of the hydrodynamic drag and inter-particle

potential on the eventual cake layer volume fraction. Therefore, the selection of models for these two quantities should be undertaken with diligence and scrutiny. Modeling the hydrodynamic drag force by Stokes law as given in Eq. (13) is historically proven and established to be correct [37]. So, attention now shifts to the inter-particle interaction, which remains an open question in terms of how to accurately model the van der Waals and electrostatic potentials. In this study, the model for the inter-particle electrostatic potential is given

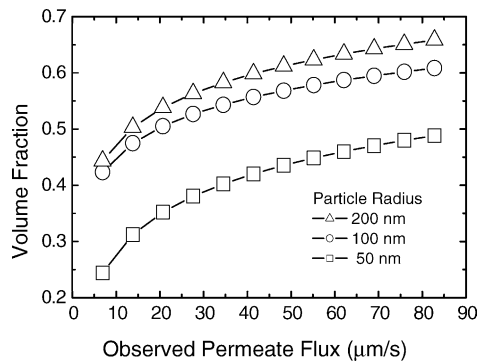


Fig. 8. Cake layer volume fraction in relation to observed permeate flux with varying particle radius. The following parameters (in addition to those listed in Table 1) were used in the simulations: zeta potential =  $-30$  mV, ionic strength =  $10^{-3}$  M.

in Eqs. (10)–(12). This model relies on using a linear superposition approximation with constant potential. Rigorous derivation and defense of this method are given in Bell et al. [25] and Chew and Sen [26].

Other expressions for electrostatic double layer interaction are available. Among them are the fundamental expressions for interactions at constant surface potential, constant surface charge, and many more other models [3,38]. A thorough discussion of the various options available is given in Chen and Kim [8].

The choice of models bears significant consequences. To further illustrate this point, a parameter  $R$  is introduced to gauge the relative magnitude of the downward hydrodynamic drag versus the inter-particle electrostatic potential:

$$R = \frac{F_{\text{hydro}}}{\Delta V_s / \Delta r} \quad (20)$$

where  $\Delta V_s$  is the difference in inter-particle potentials measured at a particle separation of 2.5 times particle radius, with a displacement  $\Delta r$  of 0.1 times particle radius. Eq. (20) essentially measures the ratio of the hydrodynamic force that the particle experiences while displacing 0.1 times particle radius in the negative  $z$ -direction towards another particle 2.5 times particle radius away versus the resistance against this displacement from the inter-particle repulsion.

Fig. 9 shows the particle volume fraction as a function of the logarithm of  $R$ . The curves exhibit two distinct regions. In region I, the particle volume fraction is an increasing function of  $\log R$ . This is an expected trend and signifies that a greater hydrodynamic drag will compress the particle configuration and generate a higher volume fraction. The model implemented in the current study according to Eqs. (10)–(12) does in fact fall within region I as supported by results given in Figs. 4, 5 and 8. However, in region II, the volume fraction becomes a decreasing function of  $\log R$ . In this case, the hydrodynamic drag has surpassed a threshold beyond which it is so strong relative to the inter-particle potential that particles coalesce rapidly with less opportunity to reorder or re-

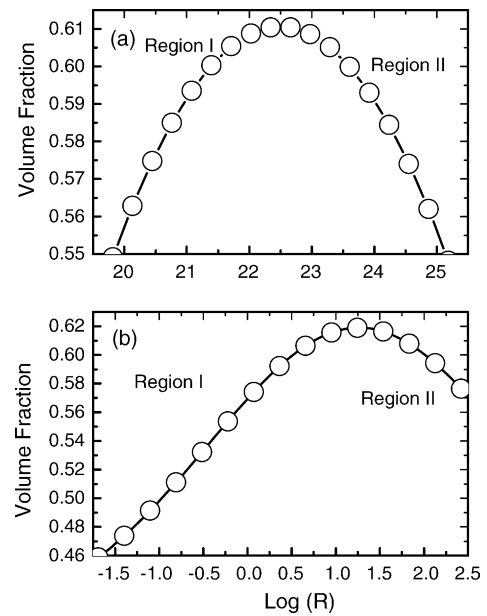


Fig. 9. Sensitivity of cake layer volume fraction to the relative magnitudes of hydrodynamic drag force vs. inter-particle potential. The following parameters (in addition to those listed in Table 1) were used in the simulations: (a) ionic strength =  $10^{-1}$ , (b) ionic strength =  $10^{-2}$ .

structure their configuration. As a result, the volume fraction decreases with increasing hydrodynamic drag. Switching to a different model for the inter-particle potential or varying the magnitude of the physical parameters inputted into the model may cause the model to shift from region I to region II or vice versa.

Fig. 9(a) and (b) also shows a comparison of the behavior of the ratio  $\log R$  in response to adjustments in the ionic strength. With a lower ionic strength of  $10^{-2}$  M in Fig. 9(b), the values of  $\log R$  decrease significantly from that of Fig. 9(a). This is because at a lower ionic strength, inter-particle repulsive interactions are stronger and therefore greatly reduces the ratio of hydrodynamic force versus inter-particle repulsion. Nevertheless, even when the inter-particle repulsions are stronger, a threshold still exists where the particle deposition dynamics will transition into a region II behavior as shown in Fig. 9(b).

Here it should be noted that a model that falls under region II does not automatically disqualify it as being incorrect. That is because of the presence of counterbalancing forces in the system that will allow for the particles to restructure into configurations of higher volume fraction. Those forces include crossflow shear and compression by gravity. The formation of the cake layer may involve a two-stage process where particles first readily deposit on the membrane surface at lower volume fractions (region II behavior) and then subsequently restructure or collapse into a final formation of high volume fraction [10]. This trend may be present in dilute bulk suspensions where particles deposit singularly onto the membrane surface. So, in a system involving a dilute bulk suspension in crossflow filtration, the dynamics of

cake formation may extend beyond a simple region I relationship between the downward hydrodynamic drag and the inter-particle potential. Therefore, the selection of models to implement should not be aimed solely at seeking a region I behavior.

What Fig. 9(a) and (b) do convey are the repercussions that result from the sensitive choice of mathematical expressions and values to input to define the system. For the model in the current study, two quantities have been identified to be paramount: hydrodynamic drag force and inter-particle potential. Which model to choose and what values to input for its physical parameters? That is among the most important questions for the development of a model that remains responsible to the true situation. The final decision should be rigorously tested against experimental observation of the actual physical parameters. The mandate for judicious selection of the model to implement appears overly obvious, and likewise, the testing of physical parameters may be relegated as mundane detail. However, these simple yet crucial steps of inspection are often overlooked in the development of model simulations.

## 5. Critical flux and phase transition

### 5.1. Definition of critical flux

In Section 4.1, one of the possible definitions for the point of phase transition from a fluid-like polarization layer to a solid cake layer has been given. It relies on the inter-particle separation distance as the defining criterion for phase transition. Phase transition is identified to be the point where particles come into contact with one another (surface-to-surface inter-particle separation equals zero). As mentioned previously, this view is intuitively clear but may not bear practical significance as it does not relate itself to the operational performance of a membrane filtration system. More pragmatic interpretations of phase transition may be formulated by integrating the concept of an observed critical flux during the filtration cycle.

Some ambiguity still remains about the exact interpretation of the critical flux [16,39–41]. The opinions of several authors, for instance Howell et al. [41], Chang et al. [1], and Chan and Chen [42], are converging in agreement to the critical flux concept introduced by Field et al. [16]. Field et al. [16] classifies the critical flux into two sub-categories, the strong and weak forms. The strong form of the critical flux states that there exists a point below which the filtration of a colloidal suspension will yield the same flux as pure water for the same applied pressure [16,17]. The weak form relaxes this stringent guideline and casts the critical flux as the point below which a linear relationship exists between the applied pressure and permeate flux. The slope of the linear relationship is allowed to differ from that of the pure-water flux [16,17]. The interpretation of Field et al. [16] will be applied here to refine the simplistic ap-

proach regarding the point of particle contact as indicating phase transition so as to arrive at a more holistic set of pragmatic criteria adaptable to various filtration operating conditions.

### 5.2. Relating critical flux to phase transition

A dead-end filtration system, shown in Fig. 1, will be modeled here. No crossflow shear occurs in the dead-end system. The only forces present are the applied pressure and inter-particle potential. For this case, a system of equations is first solved, Eq. (5) and the two equations [31]:

$$\delta_c = \left( \frac{\Delta P}{\mu r_c v_{w0}} \right) (\sqrt{1 + \alpha t} - 1), \quad \alpha = \frac{2\phi_b r_c v_{w0}}{(\phi_c - \phi_b) R_m} \quad (21)$$

Solving this set of equations will yield the system response of permeate flux as a function of applied pressure, shown in Fig. 10. For a dead-end filtration system, the particle deposit will continually build up over time, and so the system response will also vary with time of filtration (2 and 5 h). At 5 h, a thicker cake layer has accumulated and so the yield in permeate flux is lower than after 2 h of filtration.

The two forms of the critical flux are identifiable from the curves in Fig. 11. The strong form of the critical flux occurs at low applied pressures as the system response deviates from the clean water flux. For the case of  $10^{-3}$  M ionic strength and 5 h of filtration, the strong form of the critical flux occurs at applied pressure of 6.894 kPa (1 psi) (Fig. 11(a)). The volume fraction of the cake layer is 0.472 with thickness

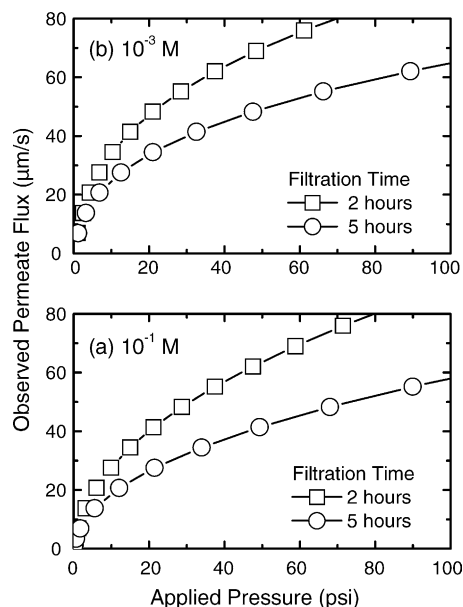


Fig. 10. Observed permeate flux as a function of applied pressure for 2 and 5 h of dead-end filtration. The following parameters (in addition to those listed in Table 1) were used in the simulations: (a) zeta potential =  $-30$  mV, ionic strength =  $10^{-1}$  M, particle radius = 100 nm; (b) zeta potential =  $-30$  mV, ionic strength =  $10^{-3}$  M, particle radius = 100 nm.

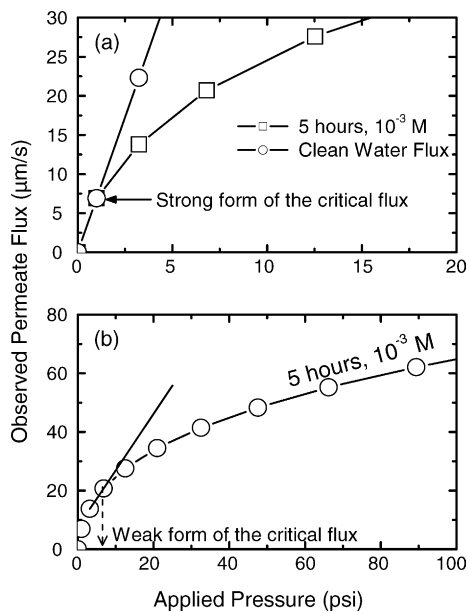


Fig. 11. Identification of the strong form of the critical flux. The following parameters (in addition to those listed in Table 1) were used in the simulations: (a) zeta potential =  $-30$  mV, ionic strength =  $10^{-3}$  M, particle radius =  $100$  nm. The volume fraction of the cake layer at the strong form of the critical flux is  $0.472$  with cake thickness  $28.6$   $\mu\text{m}$  and average center-to-center inter-particle separation distance of  $2.250$  times particle radius; (b) zeta potential =  $-30$  mV, ionic strength =  $10^{-3}$  M, particle radius =  $100$  nm. The volume fraction of the cake layer at the weak form of the critical flux is  $0.537$  with cake thickness  $136$   $\mu\text{m}$  and average inter-particle separation  $2.195$  times particle radius.

$28.6$   $\mu\text{m}$  and average center-to-center inter-particle separation distance of  $2.25$  times particle radius. There is very little basis to assign the strong form of the critical flux as the point of phase transition. First, the particles are not in contact. Second, the particle deposit does not greatly affect the system behavior (only the beginning of a deviation from the clean water flux is observed). The strong form of the critical flux fails on both fronts, the simplistic view of phase transition in terms of particle contact and the practical view in terms of operational impact. Therefore, the strong form of the critical flux only defines the presence of a fluid-like polarized layer (i.e., concentration polarization).

From Fig. 11(b), the weak form of the critical flux for the case of  $10^{-3}$  M ionic strength occurs at  $55.152$  kPa ( $8$  psi) applied pressure with volume fraction  $0.537$ , cake thickness  $136$   $\mu\text{m}$ , and average center-to-center inter-particle separation  $2.195$  times particle radius. Here again the particles are not in contact. However, a significant change in filtration behavior does occur. Once the system diverges from the linear relationship beyond the weak form of the critical flux, the filtration performance begins to decline greatly. As can be seen from Fig. 10(a) and (b), a large increase in the applied pressure after the critical flux will no longer generate nearly the comparable increase in flux as prior to the critical flux. This deterioration in productivity caused by the cake layer is commonly termed membrane fouling. It would then be

appropriate to designate this to be another possible point of phase transition. The weak form of the critical flux demarcates the onset of phase transition from concentration polarization to a particle deposit that will substantially restrict filtration performance. The particles need not be in contact; the underpinning criterion adopts a practical consideration where an incremental increase in the applied pressure will yield only limited increase in permeate flux. The rationale behind this perspective argues that the transition from a fluid to solid phase should be defined in terms of the impact on filtration performance. Once a significant decline in filtration productivity is observed, the solidification of the cake layer is deemed to occur. A summary of the strong and weak forms of the critical flux for the case of ionic strength  $10^{-3}$  M is given in Fig. 12.

### 5.3. Cake irreversibility

Finally, besides the point of particle contact and the critical flux, another alternative for defining phase transition relies on the idea of cake irreversibility [40,43,44]. After the particles come into contact, continued exertion of pressure will lead to their adhesion, which produces an irreversible cake layer. An irreversible cake layer will remain on the membrane even after a release of the applied pressure. The cake layer formed is permanent in contrast to the case of mere particle contact where the solidified deposit will disintegrate upon release of the applied pressure. The formation of an irreversible cake layer bears serious ramifications for filtration operations. A typical membrane filtration system will operate according to cycles of membrane cleaning. An irreversible cake layer may persist after the cleaning procedure and permanently exacerbate the system performance. So, another practical designation of phase transition has been recognized. *Phase transition indicates the occurrence of an irreversible cake layer where particles are in contact and adhered. The cake layer formed is permanent and will persist upon a release of pressure and may be resistant to cleaning.* This viewpoint bases its justi-

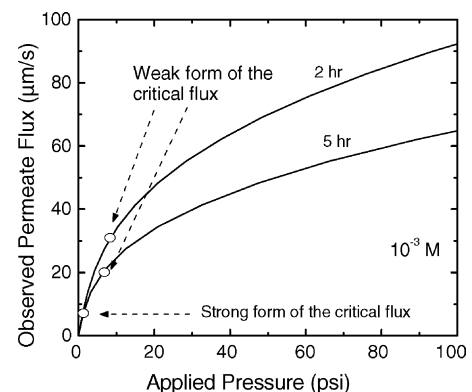


Fig. 12. Summary of the strong and weak forms of the critical flux. The following parameters (in addition to those listed in Table 1) were used in the simulations: zeta potential =  $-30$  mV, ionic strength =  $10^{-3}$  M, particle radius =  $100$  nm.

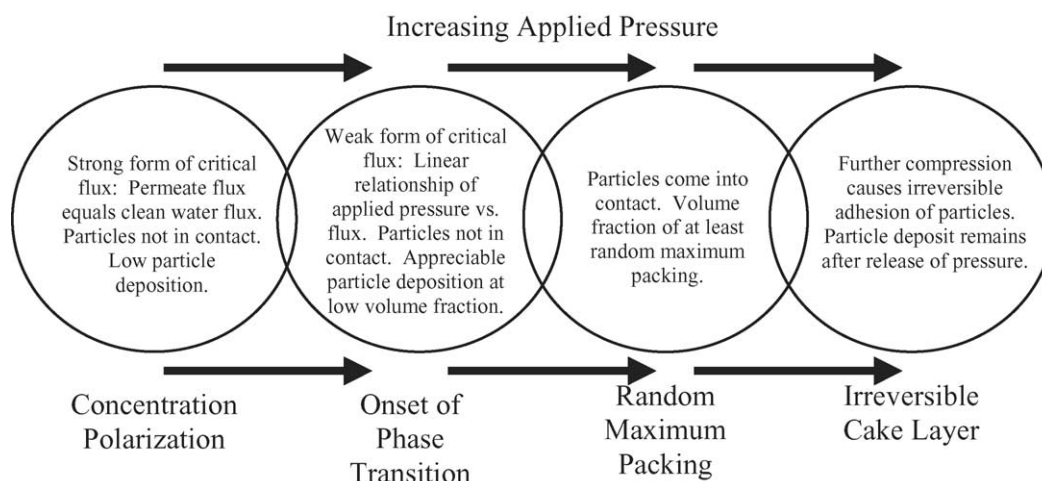


Fig. 13. Summary of the relationship between various definitions of phase transition.

fication on the idea of permanence of the phase transition. A solid phase should be enduring and not temporal in that it should remain regardless of the applied pressure, which precisely defines an irreversible cake formation.

So, a multiplicity of perspectives is available to characterize the point of phase transition from a fluid-like polarized layer to a solid cake. Fig. 13 provides a summary of these classifications. Which definition of phase transition is valid would depend on the mode of operation of the filtration system. For instance, if efficient productivity is sought, the weak form of the critical flux would be the relevant parameter for gauging phase transition. Likewise, if effective membrane cleaning is the guideline for operation, then the criterion for phase transition can be relaxed to correspond to the point of cake irreversibility. The definitions of phase transition should remain multifarious and flexible so that it can be adaptable to a vast range of operating conditions and standards of performance.

## 6. Conclusion

This study endeavors to develop a comprehensive Monte Carlo simulation of colloidal membrane filtration for the purposes of investigating the phase transition phenomenon of the particle deposit from a fluid-like polarization layer to a solid cake. Colloidal membrane filtration involves a complex array of counterworking forces acting simultaneously. The set of physical processes that govern filtration includes crossflow shear, permeation drag, inter-particle interaction potential, gravitational compression, restructuring of the deposit, particle aggregation, breakage of aggregate, and particle collisions. Such an elaborate system bewilders macroscopic modeling techniques that apply averaged values of the physical parameters and thereby lose valuable information about the inner workings of the intricate system. So, the problem of colloidal membrane filtration casts hydrodynamic bias Monte Carlo simulation as an extremely advantageous alternative that possesses the efficacy to capture the minute details of ev-

ery distinct force and particle displacement. Monte Carlo simulation has traditionally been widely accepted in the physical sciences. Among the objectives of this study is to reinforce the fledgling extension of this powerful modeling technique into membrane separation and fouling studies.

The model presented in this study has completed the preliminary stages of development. It competently models the concurrent effects of the permeation hydrodynamic drag and inter-particle interaction potential on the dynamics of particle deposition onto the membrane surface. The interplay between these two forces is shown to be among the most crucial elements that determine the physical accuracy of the model. Furthermore, the model is applied to gain insights into the phase transition phenomenon of the particle deposit. Three possible criteria for phase transition are identified—weak form of the critical flux, particle contact, and irreversible adhesion of particles. Multiple characterizations of the point of phase transition allow for incorporation of practical considerations such as filtration performance and, therefore, offer the flexibility for adaptation to a wide range of physical situations.

The current study will continue by progressively adding further considerations for the variegated array of forces and phenomena mentioned above. The model in its final form will approach a close facsimile of real systems. Many of the important topics of study in membrane filtration such as membrane fouling and locally varying dynamics of cake layer formation can be simulated by a comprehensive robust model. The outlook of the current model is optimistic with promising new developments and applications to follow.

## Acknowledgments

This research was supported by the U.S. National Science Foundation (Grant BES 0114527), the U.S. Geological Survey (Grant 01HQGR0079), through the Water Resources Research Center, University of Hawaii at Manoa, Honolulu, and Saehan Industries, Seoul, Korea.

## Nomenclature

$a$	particle radius
$a_0$	uniform random number between 0 and 1
$A_H$	Hamaker's constant
$D(\phi)$	concentration-dependent diffusion coefficient of particles
$e$	charge of an electron
$I$	ionic strength of the solution
$k_B$	Boltzmann's constant
$n_0$	ion number concentration
$N_A$	Avogadro's number
$\Delta P$	applied pressure within the system
$r_c$	specific cake resistance
$r_i^m$	particle location
$R$	parameter characterizing ratio of hydrodynamic drag to inter-particle potential
$R_c$	cake layer resistance
$R_m$	membrane resistance
$s$	dimensionless center-to-center separation
$T$	absolute temperature
$u$	crossflow velocity
$V_{EDL}$	inter-particle electrostatic potential
$V_{VDW}$	van der Waals' potential
$\Delta V_{n,m}$	change in potential energy
$z_s$	valence of ions in the bulk solution

## Greek letters

$\delta_c$	cake layer thickness
$\delta r_{\max}$	maximum allowable displacement
$\epsilon_r$	relative permittivity of water
$\epsilon_0$	permittivity of free space
$\kappa^{-1}$	Debye screening length
$\mu$	absolute dynamic fluid viscosity
$v$	permeate flux
$v_w$	permeate flux in magnitude
$\xi$	a uniform random number between 0 and 1
$\rho_n/\rho_m$	Boltzmann factor of the energy difference
$\phi$	volume fraction of particles in the cake layer
$\phi_b$	bulk volume fraction of particles
$\phi_c$	cake layer volume fraction
$\phi_m$	particle volume fraction at the membrane surface
$\psi_s$	surface potential of the particles
$\Omega$	Happel's correction factor

## References

- [1] S. Chang, A.G. Fane, S. Vigneswaran, Modeling and optimizing submerged hollow fiber membrane modules, *AIChE J.* 48 (2002) 2203–2212.
- [2] B.D. Cho, A.G. Fane, Fouling transients in nominally sub-critical flux operation of a membrane bioreactor, *J. Membr. Sci.* 209 (2002) 391–403.
- [3] W.B. Russel, D.A. Saville, W.R. Schowalter, *Colloidal Dispersions*, Cambridge University Press, New York, 1989.
- [4] R.S. Faibish, M. Elimelech, Y. Cohen, Effect of interparticle electrostatic double layer interactions on permeate flux decline in crossflow membrane filtration of colloidal suspensions: an experimental investigation, *J. Colloid Interface Sci.* 204 (1998) 77–86.
- [5] C.A. Romero, R.H. Davis, Transient model of crossflow microfiltration, *Chem. Eng. Sci.* 45 (1990) 13–25.
- [6] L.F. Song, M. Elimelech, Theory of concentration polarization cross-flow filtration, *J. Chem. Soc., Faraday Trans.* 91 (1995) 3389–3398.
- [7] A. Zydny, C.K. Colton, A concentration polarization model for the filtrate flux in cross-flow microfiltration of particulate suspensions, *Chem. Eng. Commun.* 47 (1986) 1–21.
- [8] J.C. Chen, A.S. Kim, Review of Brownian dynamics, molecular dynamics and Monte Carlo modeling of colloidal systems, *Adv. Colloid Interface Sci.* 112 (2004) 159–173.
- [9] M.P. Allen, D.J. Tildesley, *Computer Simulation of Liquids*, Clarendon Press, Oxford, UK, 1994.
- [10] V.V. Tarabara, I. Koyuncu, M.R. Wiesner, Effect of hydrodynamics and solution ionic strength on permeate flux in cross-flow filtration: direct experimental observation of filter cake cross-sections, *J. Membr. Sci.* 241 (2004) 65–78.
- [11] M.R. Mackley, N.E. Sherman, Cake filtration mechanisms in steady and unsteady flows, *J. Membr. Sci.* 77 (1993) 113–121.
- [12] G. Green, G. Belfort, Fouling of ultrafiltration membranes: lateral migration and the particle trajectory model, *Desalination* 35 (1980) 129–147.
- [13] A.G. Fane, Ultrafiltration of suspensions, *J. Membr. Sci.* 20 (1984) 249–259.
- [14] V.V. Tarabara, F. Pierrisnard, C. Parron, J.-Y. Bottero, M.R. Wiesner, Morphology of deposits formed from chemically heterogeneous suspensions: application to membrane filtration, *J. Colloid Interface Sci.* 256 (2002) 367–377.
- [15] J.C. Chen, Q. Li, M. Elimelech, In situ monitoring techniques for concentration polarization and fouling phenomena in membrane filtration, *Adv. Colloid Interface Sci.* 107 (2004) 83–108.
- [16] R.W. Field, D. Wu, J.A. Howell, B.B. Gupta, Critical flux concept for microfiltration fouling, *J. Membr. Sci.* 100 (1995) 259–272.
- [17] D. Wu, J.A. Howell, R.W. Field, Critical flux measurement for model colloids, *J. Membr. Sci.* 152 (1999) 89–98.
- [18] C.A. Romero, R.H. Davis, Global model of crossflow microfiltration based on hydrodynamic particle diffusion, *J. Membr. Sci.* 39 (1988) 157–185.
- [19] S. Bhattacharjee, A.S. Kim, M. Elimelech, Concentration polarization of interacting solute particles in cross-flow membrane filtration, *J. Colloid Interface Sci.* 212 (1999) 81–99.
- [20] S. Sethi, M.R. Wiesner, Modeling of transient permeate flux in cross-flow membrane filtration incorporating multiple particle transport mechanisms, *J. Membr. Sci.* 136 (1997) 191–205.
- [21] J. Happel, Viscous flow in multiparticle systems: slow motion of fluids relative to beds of spherical particles, *AIChE J.* 4 (1958) 197–201.
- [22] B.V. Derjaguin, L.D. Landau, Theory of the stability of strongly charged lyophobic sols and of the adhesion of strongly charged particles in solutions of electrolytes, *Acta Physicochim. URSS* 14 (1941) 733–762.
- [23] E.J. Verwey, J.T.G. Overbeek, *Theory of the Stability of Lyophobic Colloids*, Elsevier, Amsterdam, 1948.
- [24] H.C. Hamaker, The London-van der Waals attraction between spherical particles, *Physica* 4 (1937) 1058–1072.
- [25] G.M. Bell, S. Levine, L.N. McCartney, Approximate methods of determining the double-layer free energy of interaction between two charged colloidal spheres, *J. Colloid Interface Sci.* 33 (1970) 335–359.
- [26] W.C. Chew, P.N. Sen, Potential of a sphere in an ionic solution in thin double layer approximations, *J. Chem. Phys.* 77 (1982) 2042–2044.

- [27] W.R. Bowen, F. Jenner, Dynamic ultrafiltration model for charged colloidal dispersions: a Wigner-Seitz cell approach, *Chem. Eng. Sci.* 50 (1995) 1707–1736.
- [28] N. Metropolis, A.W. Rosenbluth, M.N. Rosenbluth, A.H. Teller, E. Teller, Equation of state calculations by fast computing machines, *J. Chem. Phys.* 21 (1953) 1087–1092.
- [29] W.K. Hastings, Monte Carlo sampling methods using Markov chains and their applications, *Biometrika* 57 (1970) 97–109.
- [30] V.I. Manousiouthakis, M.W. Deem, Strict detailed balance is unnecessary in Monte Carlo simulation, *J. Chem. Phys.* 110 (1999) 2753–2756.
- [31] A.S. Kim, E.M.V. Hoek, Cake structure in dead-end membrane filtration: Monte Carlo simulation, *Environ. Eng. Sci.* 19 (2002) 373–386.
- [32] A.S. Kim, S. Bhattacharjee, M. Elimelech, Shear-induced reorganization of deformable molecular assemblages: Monte Carlo studies, *Langmuir* 17 (2001) 552–561.
- [33] G.Y. Onoda, E.G. Liniger, Random loose packing of uniform spheres and the dilatancy onset, *Phys. Rev. Lett.* 64 (1990) 2727–2730.
- [34] R.M. McDonogh, A.G. Fane, C.J.D. Fell, H.-C. Flemming, The influence of polydispersity on the hydraulic behaviour of colloidal fouling layers on membranes: perturbations on the behaviour of the “ideal” colloidal layer, *Colloids Surf. A: Physicochem. Eng. Aspects* 138 (1998) 231–244.
- [35] T. Bahners, E. Schollmeyer, Computer simulation of the filtration process in a fibrous filter collecting polydisperse dust, *J. Aerosol Sci.* 17 (1986) 191–197.
- [36] M.R. Mackley, N.E. Sherman, Cross-flow filtration with and without cake formation, *Chem. Eng. Sci.* 49 (1994) 171–178.
- [37] E.R. Damiano, D.S. Long, F.H. El-Khatib, T.M. Stace, On the motion of a sphere in a Stokes flow parallel to a Brinkman half-space, *J. Fluid Mech.* 500 (2004) 75–101.
- [38] M. Elimelech, J. Gregory, X. Jia, W. Williams, *Particle Deposition and Aggregation: Measurement, Modeling, and Simulation*, Butterworths/Heinemann, Oxford, 1995.
- [39] P. Bacchin, P. Aimar, V. Sanchez, Model for colloidal fouling of membranes, *AIChE J.* 41 (1995) 368–376.
- [40] P. Bacchin, A possible link between critical and limiting flux for colloidal systems: consideration of critical deposit formation along a membrane, *J. Membr. Sci.* 228 (2004) 237–241.
- [41] J.A. Howell, T.C. Arnot, H.C. Chua, P. Godino, D. Hatziantoniou, S. Metsamuuronen, Controlled flux behaviour of membrane processes, *Macromol. Symp.* 188 (2002) 23–35.
- [42] R. Chan, V. Chen, The effects of electrolyte concentration and pH on protein aggregation and deposition: critical flux and constant flux membrane filtration, *J. Membr. Sci.* 185 (2001) 177–192.
- [43] S. Metsamuuronen, J. Howell, M. Nystrom, Critical flux in ultrafiltration of myoglobin and baker’s yeast, *J. Membr. Sci.* 196 (2002) 13–25.
- [44] V. Chen, A.G. Fane, S. Madaeni, I.G. Wenten, Particle deposition during membrane filtration of colloids: transition between concentration polarization and cake formation, *J. Membr. Sci.* 125 (1997) 109–122.